Liu et al. Nanoscale Research Letters (2019) 14:284
https://doi.org/10.1186/s11671-019-3120-x

Nanoscale Research Letters

NANO EXPRESS Open Access

Solution-Processed Inorganic Perovskite Flexible Photodetectors with High Performance

Ziji Liu†, Hao Li†, Chaojie Qin, Ting Zhang, Yiding Gu, Hao Chen, Hualin Zheng and Shibin Li*

Abstract

All inorganic $CsPbI_{3-x}Br_x$ perovskites have been widely used in photodetectors due to their excellent optoelectronic properties and simple preparation processes. Here, high-performance flexible photodetectors based on inorganic $CsPbI_{3-x}Br_x$ perovskites are demonstrated, which are achieved by a modified solution-processed method. When biased at a low voltage of 10 mV, the device yielded fast response speeds (90 μs /110 μs for $CsPbI_2Br$ PDs and 100 μs/140 μs for $CsPbIBr_2$ PDs), a high on/off ratio of 10^4, and a high detectivity about 10^{12} Jones. Meanwhile, the devices showed outstanding environmental stability and mechanical flexibility. The periodic I-t curves had negligible fluctuation (< 5%) after storing in air atmosphere for 30 days or bending for 100 times. The results indicate that $CsPbI_{3-x}Br_x$ perovskites have great potential in photodetection areas and pave the way to achieve high-performance flexible PDs.

Keywords: $CsPbI_{3-x}Br_x$-based flexible PDs, Low bias voltage, Environmental stability, Mechanical flexibility

Introduction

In the past few decades, a variety of inorganic semiconductor materials have drawn most attention of photodetectors research, such as InGaAs, GaN, ZnO, and Si [1–6]. Benefited by their excellent optical and electrical properties, the devices based on these materials exhibit high detectivity and fast response for visible light. However, such materials are usually obtained by extremely complex approaches or using expensive equipment [7–9], which is a bottleneck on the way to their commercial application. Hence, seeking for more promising substitute materials to reduce the cost, and simplify the preparation process is very important.

Recently, hybrid halide perovskites (HHPs) materials have been one of the research hot spots in the field of photovoltaic devices [10–15]. In the last decade, the power conversion efficiencies of perovskite solar cells have been increased from 3.8% to exceed 23% [16–27], owing to its remarkable optoelectronic properties, such as the merits of the optimum bandgap, high absorption coefficient, and superior ambipolar carrier transport ability [28–31]. In addition, low-cost and simple solution process preparation also makes perovskites have great potential in the research of photodetectors. However, in spite of the photovoltaic devices based on HHPs have made rapid and impressive progress, they still suffer from poor stability [32, 33]. Compared with HHPs, inorganic cesium lead halide perovskites (IHPs) exhibit better stability in the air, indicating that IHPs is an ideal candidate for photodetectors [34, 35]. Although, $CsPbI_3$ is unstable at high temperature (above 300 °C), which can be improved by substituting the Br^- moiety for I^- [36–41]. Therefore, $CsPbI_{3-x}Br_x$ is very suitable for designing high-performance photodetectors.

In this work, we prepared $CsPbI_{3-x}Br_x$ ($x = 1, 2$) films for flexible perovskite photodetectors (PDs). The flexible perovskite PDs based on $CsPbI_{3-x}Br_x$ exhibited fast response speed (90 μs/110 μs for $CsPbI_2Br$ PDs and 100 μs/140 μs for $CsPbIBr_2$ PDs), a high on/off ratio (10^4), and a high detectivity (10^{12} Jones) under 520 nm lamp with 10 mV bias. Meanwhile, it exhibited outstanding mechanical flexibility and environmental stability. After keeping the device for 30 days in ambient air at 35–45% relative humidity, the periodic I-t curves of the device are only slightly declined (~ 3%). In addition, after bending the flexible PDs for 100 times under the bending radius of 9.12 mm, the periodic I-t curves of the device showed negligible change (< 3%

* Correspondence: shibinli@uestc.edu.cn
†Ziji Liu and Hao Li contributed equally to this work.
State Key Laboratory of Electronic Thin Films and Integrated Devices, and School of Optoelectronic Science and Engineering, University of Electronic Science and Technology of China (UESTC), Chengdu 610054, Sichuan, China

decrease). The results indicate the potential of $CsPbI_{3-x}Br_x$ perovskites for flexible PDs.

Method

Materials

Lead iodide (PbI_2, 99.99%), lead bromide ($PbBr_2$, 99.99%), barium iodide (CsI, 99.99%), and barium bromide (CsBr, 99.99%) were purchased from Xi'an Polymer Light Technology Corporation. Diethyl ether (DEE), acetone, absolute ethanol, *N*,*N*-dimethylformamide (DMF), and dimethylsulfoxide (DMSO) were provided by Sigma-Aldrich.

The perovskite solution was prepared as follows. The $CsPbI_2Br$ perovskite precursor solutions were prepared by mixing the 1 M (mol L^{-1}) CsBr, 1 M $PbBr_2$, 2 M CsI, and 2 M PbI_2 in mixed anhydrous solvents of DMSO and DMF (9:1 in volume). The $CsPbIBr_2$ perovskite precursor solutions were prepared by mixing the 2 M CsBr, 2 M $PbBr_2$, 1 M CsI, and 1 M PbI_2 in mixed anhydrous solvents of DMSO and DMF (9:1 in volume). Then, the mixed perovskite solutions were stirred at 75 °C more than 2 h. All solutions must be were prepared in a nitrogen glovebox.

Preparation

Flexible substrates [polyimide (PI)] were cleaned consecutively with acetone, absolute ethanol, and deionized water for 15 min, respectively. And then the substrates were dried in an oven. Subsequently, interdigitated golden electrode (80 nm) was evaporated onto the flexible substrates by thermal evaporation. Before use, the patterned substrates were treated with UV-ozone for 20 min. Then the flexible substrates were transferred into glovebox for perovskite films deposition. The $CsPbI_{3-x}Br_x$ films were prepared using anti-solvent (DEE) one-step spin-coating method. Eighty-microliter precursor solution was spin-coating at a speed of 2000 rpm for 60 s. Then, 0.5 mL diethyl ether was poured on the samples at 10 s before the end of the spinning-coating processes. Then, the samples were annealed at 65 °C for 5 min and 135 °C for 15 min.

Measurements and Characterizations

Scanning electron microscope (SEM) images were obtained by using field emission SEM (FEI- INSPECT F50, Holland). X-ray diffraction (XRD) was carried out using a Bede D1 system with Cu Kα radiation. The ultraviolet-visible (UV-vis) absorption spectrum was measured by an UV-vis spectrophotometer (Schimadzu UV-3101 PC). The current–voltage (*I-V*) curves were carried out by Keithley 2636 semiconductor parametric analyzer under the illumination of a LD light source. Photocurrent was measured with an oscilloscope (Agilent DOS5012A) and an optical chopper modulating the light illuminated on the device. All measurements were carried out under ambient conditions at room temperature.

Results and Discussion

Anti-solvents, which are often used in the preparation of perovskite films to obtain a high-quality surface morphology. Herein, we used one-step spin-coating method with anti-solvent (DEE) to improve the morphology of $CsPbI_{3-x}Br_x$ films. Figure 1 exhibits the plan-view SEM images of $CsPbI_{3-x}Br_x$ films with or without DEE treatment. As shown in Fig. 1a, b, the $CsPbI_2Br$ and $CsPbIBr_2$ film without DEE-treatment possess enormous pinholes and small crystal grain size. In contrast, after DEE-treatment in the fabrication of perovskite, continuous film and larger grains are observed in the SEM images (Fig. 1c, d). The results of SEM images indicated that the morphology of the $CsPbI_{3-x}Br_x$ films was significantly improved by the treatment of DEE. Therefore, in the subsequent work, the anti-solvent treatment process was adopted to prepare $CsPbI_{3-x}Br_x$ films.

In order to examine the crystal structure of the prepared $CsPbI_{3-x}Br_x$ films, XRD patterns were carried out. As shown in Fig. 2a, the red and the blue lines indicate the XRD patterns of $CsPbIBr_2$ films and $CsPbI_2Br$, respectively. It was clear to observe, in the red lines, the main peaks located at 14.75°, 20.94°, 29.96°, and 34.93°, which are assigned to the (100), (110), (200), and (210) facts of $CsPbIBr_2$, respectively [41–43]. In the blue lines, we note two main peaks centered at 14.44° and 20.3° corresponding to the (100) and (200) planes of the pure $CsPbI_2Br$ α phase [44, 45]. In addition, to certify that the $CsPbIBr_2$ and $CsPbI_2Br$ films were successfully prepared, UV-vis absorption curves and Tauc plots were measured (Fig. 2b–d). As shown in Fig. 2b, a small blue shift is visible in the absorption spectrum of the $CsPbIBr_2$ film compared to the $CsPbI_2Br$ film, which attributed to the bandgap difference between $CsPbI_2Br$ and $CsPbIBr_2$. To explore the optical bandgap of $CsPbI_{3-x}Br_x$ film, we calculated the energy band (Eg) according to the reflection and transmission through the Tauc plots, as shown in Fig. 2c, d. It was observed from the Tauc plots that Eg of $CsPbI_2Br$ and $CsPbIBr_2$ were 1.91 eV and 2.05 eV, respectively, which is consistent with the previous report [46–50]. The results indicated the $CsPbI_{3-x}Br_x$ films were successfully fabricated.

After confirming the properties of the treated $CsPbI_{3-x}Br_x$ films, we prepared the flexible PDs based on $CsPbI_{3-x}Br_x$ films. In Fig. 3a, the flexible PDs with the device structure of PI/Au interdigitated electrodes/$CsPbI_{3-x}Br_x$ are shown. When it is irradiated on the perovskite layer under a bias voltage, the charge carrier transport is formed in PDs, as shown in Fig. 3b. Finally, electrons (holes) are collected by electrodes and circulated through an external circuit to generate photocurrent. To characterize the performance of $CsPbI_{3-x}Br_x$ PDs, we measured the photocurrent under 520 nm LD source at low bias voltages as shown in Fig. 3c, d. The result showed that the maximum photocurrent of $CsPbI_2Br$ PDs and $CsPbIBr_2$ PDs were beyond 180 μA and

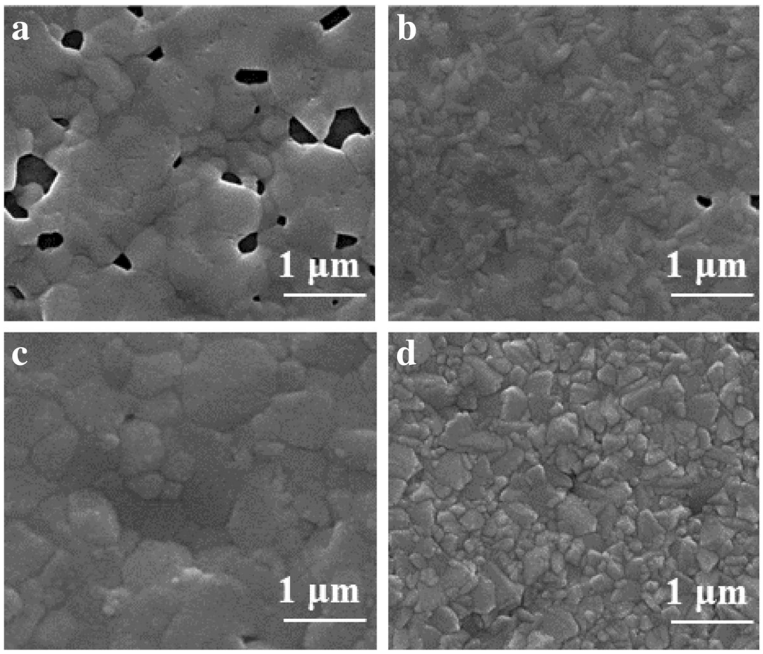

Fig. 1 SEM image of the $CsPbI_{3-x}Br_x$ films. **a** $CsPbI_2Br$, **b** $CsPbIBr_2$ without DEE treatment and **c** $CsPbI_2Br$, **d** $CsPbIBr_2$ with DEE treatment

120 μA under the illumination intensity of 8.23 mW/cm^2, respectively. Importantly, the photocurrent of the device was measured at a bias voltage of 10 mV. To evaluate the response speed of the device, we investigated the transient photocurrent of the device. As shown in Fig. 3c, d, the rise and decay time of $CsPbI_2Br$ PDs are extracted to be around 90 μs and 110 μs, respectively. The rise and decay time of $CsPbIBr_2$ PDs were found to be about 100 μs and 140 μs, respectively. Compared to the same structural devices previously reported [12], the results manifested that the device

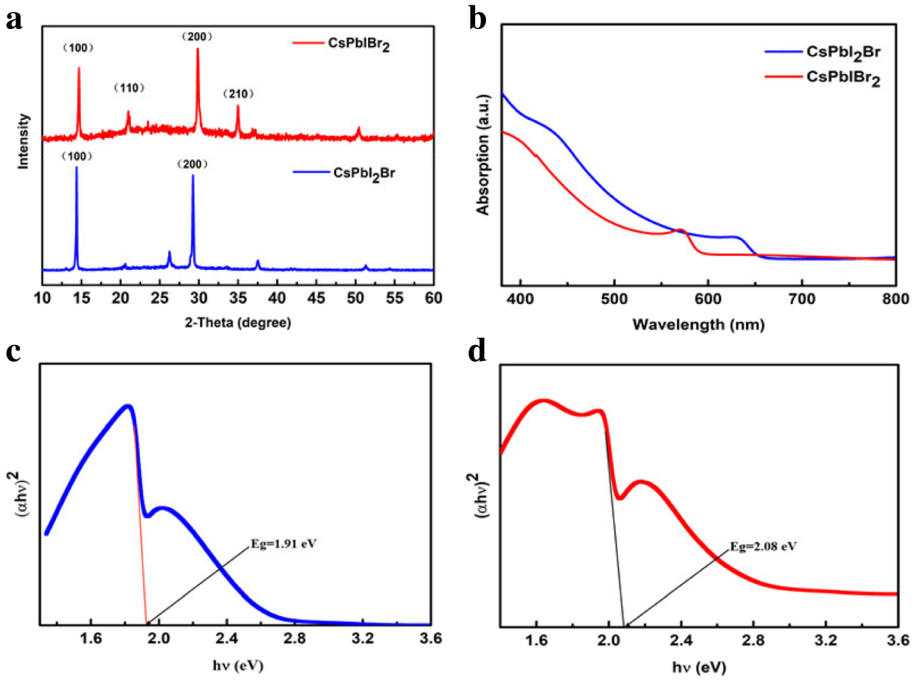

Fig. 2 **a** XRD patterns. **b** Absorption of the $CsPbI_{3-x}Br_x$ films. The band gap of **c** $CsPbI_2Br$ and **d** $CsPbIBr_2$

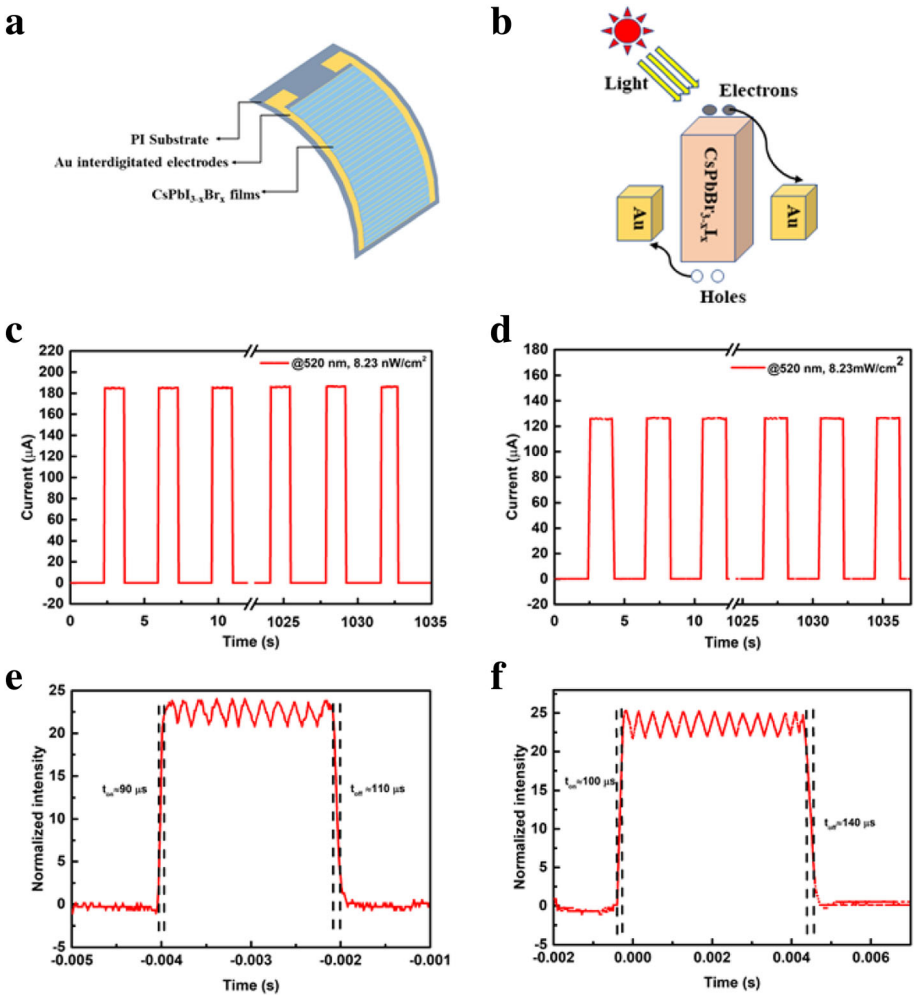

Fig. 3 **a** Device structure of the $CsPbI_{3-x}Br_x$ flexible PDs. **b** Schematic diagram of charge carrier transport in the device under illumination. I–t curves of the **c** $CsPbI_2Br$ PDs and **d** CsPbIBr2 PDs upon 520 nm light at a bias of 10 mV. The rise time (ton) and fall time (toff) of **e** $CsPbI_2Br$ PDs and **f** $CsPbIBr_2$ PDs, respectively

based on DEE-treated $CsPbI_{3-x}Br_x$ perovskite layer showed excellent performance.

To further investigate the photoelectrical characteristics of the PDs, the dark current and photo-current, responsivity, and detectivity were measured and plotted, as shown in Fig. 4. As showed in Fig. 4a, b, the dark current and photocurrent curves have approximate symmetry when the voltage was changed from − 5 to 5 V. This result indicated the formation of an ohmic contact between the metal and the perovskite layer. Owing to the contact barrier being very low for ohmic contact, carriers can be easily transferred under low bias. At low bias voltages, the $CsPbI_{3-x}Br_x$ flexible PDs possess a high on/off ratio of approximately 10^4. Responsivity (R) and detectivity (D^*) of the PDs were showed in Fig. 4c, d. The image illustrated that the R and D^* had high values under weak light at low bias, especially below 1 mW, along with a high D^* of 10^{12} Jones@10 mV bias. Zhang et al. reported a $CsPbBr_3$-based flexible PDs with a D^* of 10^{10} Jones under 2 V bias [12]. Ding et al. reported a rigid PDs based on $CsPbBr_3$ single crystals with a D^* of 10^{11} Jones [51]. Therefore, the $CsPbI_{3-x}Br_x$-based flexible PDs working under low bias voltages exhibit outstanding performances.

Environmental stability and mechanical flexibility are two important factors that influence the practical application of photodetectors based on perovskite. As described in Fig. 5, the environmental stability and mechanical flexibility of the PDs were tested by measuring the changes in periodic I-t curves of the device. It was clearly observed that the I-t curves of the device changed slightly (~ 3% decrease for $CsPbI_2Br$ PDs and ~ 3% decrease for $CsPbIBr_2$ PDs). The changes of the devices' currents could be ignored after being exposed for 30 days in ambient conditions at 35–45% relative humidity (Fig. 5a, b). As showed in Fig. 5c, d, compared with the initial periodic I-t curves,

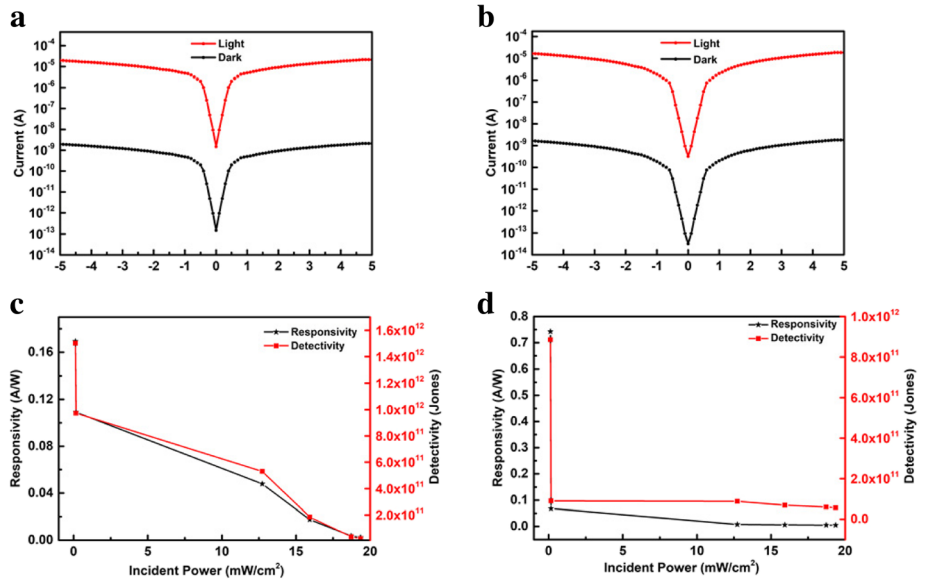

Fig. 4 The curves (I-V) of **a** $CsPbI_2Br$ PDs and **b** $CsPbIBr_2$ PDs for photocurrent (520 nm LD) and dark current. The responsivity and detectivity (illustration) of the **c** $CsPbI_2Br$ PDs and **d** $CsPbIBr_2$ PDs (520 nm LD) under 10 mV voltage

a negligible oscillation was observed (~ 2% decrease for $CsPbI_2Br$ PDs and ~ 3% decrease for $CsPbIBr_2$ PDs) after bending the device for one hundred times under the bending radius of 9.12 mm. The results demonstrate that our device has a great stability as well as good mechanical flexibility.

Conclusion

In summary, we present the flexible photodetectors based on $CsPbI_{3-x}Br_x$ ($x = 1, 2$) films which were treated with DEE in this work. The devices showed excellent performance, which were comparable to the same configuration devices. At a bias of 10 mV, the photodetectors showed a

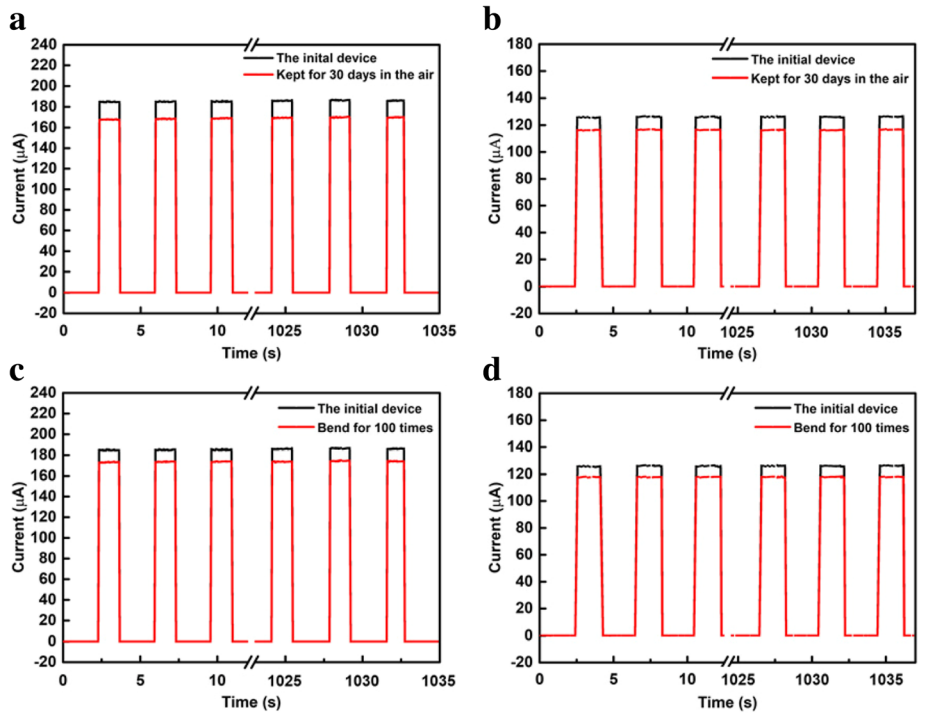

Fig. 5 Comparison of the reproducible I-t curves of **a** $CsPbI_2Br$ PDs and **b** $CsPbIBr_2$ PDs kept in air for 30 days. Comparison of the reproducible I-t curves of **c** $CsPbI_2Br$ PDs and **d** $CsPbIBr_2$ PDs bending for 100 times

high on/off ratio of 10^4 under 520 nm illumination, fast response speed (90 μs/110 μs for $CsPbI_2Br$ PDs and 100 μs/140 μs for $CsPbIBr_2$ PDs), and an excellent detectivity (10^{12} Jones). Furthermore, the flexible PDs exhibited outstanding environmental stability and mechanical flexibility. After storing the device for 30 days in air at 35–45% relative humidity, the I-t curves of the device are only slightly declined (~ 3%). In addition, performance of the PDs showed a negligible change after bending the flexible PD a hundred times with a bend radius of 9.12 mm. This work demonstrates the enormous potential of $CsPbI_{3-x}Br_x$ perovskites in photoelectron detection and provides a promising approach to achieving high performance.

Abbreviations

DEE: Diethyl ether; DMF: *N*,*N*-dimethylformamide; DMSO: Dimethylsulfoxide; HHPs: Hybrid halide perovskites; IHPs: Inorganic cesium lead halide perovskites; PDs: Photodetectors; SEM: Scanning electron microscope; UV-vis: Ultraviolet-visible; XRD: X-ray diffraction

Acknowledgements

This work was supported by the National Natural Science Foundation of China under Grant Nos. 61421002, 61874150 and 61574029.

Authors' Contributions

ZL, HL, and CQ designed and carried out the experiments. HL, CQ, TZ, and YG participated in the work to analyze the data and prepared the manuscript initially. HC and HZ polished the English. SL gave equipment support. All authors read and approved the final manuscript.

Funding

National Natural Science Foundation of China: 61421002, 61874150, and 61574029.

Availability of Data and Materials

The datasets used and/or analyzed during the current study are obtained from the corresponding author on reasonable request.

Competing Interests

The authors declare that they have no competing interests.

Received: 13 July 2019 Accepted: 8 August 2019
Published online: 17 August 2019

References

1. Kojima A, Teshima K, Shirai Y et al (2009) Organometal halide perovskites as visible-light sensitizers for photovoltaic cells [J]. J Am Chem Soc 131(17):6050–6051
2. Wang L, Jie J, Shao Z et al (2015) MoS2/Si heterojunction with vertically standing layered structure for ultrafast, high-detectivity, self-driven visible–near infrared photodetectors. Adv Funct Mater 25(19):2910–2919
3. Zhang T, Liu B, Ahmad W et al (2017) Optical and electronic properties of femtosecond laser-induced sulfur-hyperdoped silicon N+/P photodiodes. Nanoscale Res Lett 12(1):522
4. Wang H, Kim DH (2017) Perovskite-based photodetectors: materials and devices. Chem Soc Rev 46(17):5204–5236
5. Chen S, Shen L, van Aken PA et al (2017) Dual-functionalized double carbon shells coated silicon nanoparticles for high performance lithium-ion batteries. Adv Mater 29(21):1605650
6. Fang Y, Dong Q, Shao Y et al (2015) Highly narrowband perovskite single-crystal photodetectors enabled by surface-charge recombination. Nat Photonics 9(10):679
7. Gong X, Tong M, Xia Y et al (2009) High-detectivity polymer photodetectors with spectral response from 300 nm to 1450 nm [J]. Science 325(5948):1665–1667
8. Baeg KJ, Binda M, Natali D et al (2013) Organic light detectors: photodiodes and phototransistors [J]. Adv Mater 25(31):4267–4295
9. Guo Y, Liu C, Tanaka H et al (2015) Air-stable and solution-processable perovskite photodetectors for solar-blind UV and visible light. J Phys Chem Lett 6(3):535–539
10. Zhang T, Wu J, Zhang P et al (2018) High speed and stable solution-processed triple cation perovskite photodetectors. Advanced Optical Materials 6(13):1701341
11. Wang Y, Zhang Y, Lu Y et al (2015) Hybrid graphene–perovskite phototransistors with ultrahigh responsivity and gain [J]. Advanced Optical Materials 3(10):1389–1396
12. Zhang T, Wang F, Zhang P et al (2019) Low-temperature processed inorganic perovskites for flexible detectors with a broadband photoresponse. Nanoscale 11(6):2871–2877
13. Qian C, Sun J, Kong LA et al (2017) High-performance organic heterojunction phototransistors based on highly ordered copper phthalocyanine/para-sexiphenyl thin films [J]. Adv Funct Mater 27(6):1604933
14. Yantara N, Bhaumik S, Yan F et al (2015) Inorganic halide perovskites for efficient light-emitting diodes. J Phys Chem Lett 6(21):4360–4364
15. Hu W, Huang W, Yang S et al (2017) High-performance flexible photodetectors based on high-quality perovskite thin films by a vapor–solution method [J]. Adv Mater 29(43):1703256
16. Lee MM, Teuscher J, Miyasaka T et al (2012) Efficient hybrid solar cells based on meso-superstructured organometal halide perovskites. Science 338(6107):643–647
17. Li S, Zhang P, Chen H et al (2017) Mesoporous PbI2 assisted growth of large perovskite grains for efficient perovskite solar cells based on ZnO nanorods [J]. J Power Sources 342:990–997
18. Burschka J, Pellet N, Moon SJ et al (2013) Sequential deposition as a route to high-performance perovskite-sensitized solar cells [J]. Nature 499(7458):316
19. Zhang P, Wu J, Zhang T et al (2018) Perovskite solar cells with ZnO electron-transporting materials. Adv Mater 30(3):1703737
20. Yang WS, Park BW, Jung EH et al (2017) Iodide management in formamidinium-lead-halide–based perovskite layers for efficient solar cells. Science 356(6345):1376–1379
21. Cai B, Xing Y, Yang Z et al (2013) High performance hybrid solar cells sensitized by organolead halide perovskites. Energy Environ Sci 6(5):1480–1485
22. Li S, Zhang P, Wang Y et al (2017) Interface engineering of high efficiency perovskite solar cells based on ZnO nanorods using atomic layer deposition. Nano Res 10(3):1092–1103
23. Chen Y, Yang Z, Wang S et al (2018) Design of an inorganic mesoporous hole-transporting layer for highly efficient and stable inverted perovskite solar cells. Adv Mater 30(52):1805660
24. Ji L, Zhang X, Zhang T et al (2019) Band alignment of Pb–Sn mixed triple cation perovskites for inverted solar cells with negligible hysteresis. J Mater Chem A 7(15):9154–9162
25. Wang P, Wu Y, Cai B, Ma Q, Zheng X, Zhang WH (2019). Solution-Processable Perovskite Solar Cells toward Commercialization: Progress and Challenges. Adv Funct Mater. p. 1807661.
26. Wang F, Zhang T, Wang Y et al (2019) Steering the crystallization of perovskites for high-performance solar cells in ambient air. J Mater Chem A 7(19):12166–12175
27. Jeon NJ, Na H, Jung EH et al (2018) A fluorene-terminated hole-transporting material for highly efficient and stable perovskite solar cells [J]. Nat Energy 3(8):682
28. Leijtens T, Stranks SD, Eperon GE et al (2014) Electronic properties of meso-superstructured and planar organometal halide perovskite films: charge trapping, photodoping, and carrier mobility. ACS Nano 8(7):7147–7155
29. Gu X, Wang Y, Zhang T et al (2017) Enhanced electronic transport in Fe 3+-doped TiO_2 for high efficiency perovskite solar cells [J]. J Mater Chem C 5(41):10754–10760
30. Saidaminov MI, Haque MA, Almutlaq J et al (2017) Inorganic lead halide perovskite single crystals: phase-selective low-temperature growth, carrier transport properties, and self-powered photodetection. Advanced Optical Materials 5(2):1600704
31. Liu D, Li S, Zhang P et al (2017) Efficient planar heterojunction perovskite solar cells with Li-doped compact TiO2 layer. Nano Energy 31:462–468
32. Tong X, Lin F, Wu J et al (2016) High performance perovskite solar cells. Advanced Science 3(5):1500201
33. Zhao Y, Zhu K (2016) Organic–inorganic hybrid lead halide perovskites for optoelectronic and electronic applications. Chem Soc Rev 45(3):655–689
34. Zhang J, Wang Q, Zhang X et al (2017) High-performance transparent ultraviolet photodetectors based on inorganic perovskite CsPbCl 3 nanocrystals. RSC Adv 7(58):36722–36727
35. Zhang X, Wang Q, Jin Z et al (2017) Stable ultra-fast broad-bandwidth photodetectors based on α-CsPbI 3 perovskite and NaYF 4: Yb, Er quantum dots. Nanoscale 9(19):6278–6285

36. Eperon GE, Paterno GM, Sutton RJ et al (2015) Inorganic caesium lead iodide perovskite solar cells. J Mater Chem A 3(39):19688–19695
37. Zhang Y, Liu Y, Li Y et al (2016) Perovskite CH 3 NH 3 Pb (BrxI1− x) 3 single crystals with controlled composition for fine-tuned bandgap towards optimized optoelectronic applications. J Mater Chem C 4(39):9172–9178
38. Yan L, Xue Q, Liu M et al (2018) Interface engineering for all-inorganic CsPbI2Br perovskite solar cells with efficiency over 14%. Adv Mater 30(33): 1802509
39. Chen CY, Lin HY, Chiang KM et al (2017) All-vacuum-deposited stoichiometrically balanced inorganic cesium lead halide perovskite solar cells with stabilized efficiency exceeding 11%. Adv Mater 29(12):1605290
40. Wang P, Zhang X, Zhou Y et al (2018) Solvent-controlled growth of inorganic perovskite films in dry environment for efficient and stable solar cells. Nat Commun 9(1):2225
41. Sutton RJ, Eperon GE, Miranda L et al (2016) Bandgap-tunable cesium lead halide perovskites with high thermal stability for efficient solar cells. Adv Energy Mater 6(8):1502458
42. Liu C, Li W, Chen J et al (2017) Ultra-thin MoOx as cathode buffer layer for the improvement of all-inorganic CsPbIBr2 perovskite solar cells. Nano Energy 41:75–83
43. Ma Q, Huang S, Wen X et al (2016) Hole transport layer free inorganic CsPbIBr2 perovskite solar cell by dual source thermal evaporation. Adv Energy Mater 6(7):1502202
44. Beal RE, Slotcavage DJ, Leijtens T et al (2016) Cesium lead halide perovskites with improved stability for tandem solar cells. J Phys Chem Lett 7(5):746–751
45. Lau CFJ, Zhang M, Deng X et al (2017) Strontium-doped low-temperature-processed CsPbI2Br perovskite solar cells. ACS Energy Letters 2(10):2319–2325
46. Lau CFJ, Deng X, Ma Q et al (2016) CsPbIBr2 perovskite solar cell by spray-assisted deposition. ACS Energy Letters 1(3):573–577
47. Zeng Q, Zhang X, Liu C et al (2019) Inorganic CsPbI2Br perovskite solar cells: the progress and perspective. Solar RRL 3(1):1800239
48. Dong C, Han X, Zhao Y et al (2018) A green anti-solvent process for high performance carbon-based CsPbI2Br all-inorganic perovskite solar cell. Solar RRL 2(9):1800139
49. Yin G, Zhao H, Jiang H et al (2018) Precursor engineering for all-inorganic CsPbI2Br perovskite solar cells with 14.78% efficiency. Adv Funct Mater 28(39):1803269
50. Wang Y, Zhang T, Xu F et al (2018) A facile low temperature fabrication of high performance CsPbI2Br all-inorganic perovskite solar cells. Solar RRL 2(1):1700180
51. Ding J, Du S, Zuo Z et al (2017) High detectivity and rapid response in perovskite CsPbBr3 single-crystal photodetector. J Phys Chem C 121(9): 4917–4923

Publisher's Note